IEEE Access
Multidisciplinary | Rapid Review | Open Access Journal

Received May 23, 2020, accepted June 11, 2020, date of publication June 16, 2020, date of current version July 1, 2020.

Digital Object Identifier 10.1109/ACCESS.2020.3002768

Prediction of the Cement Grate Cooler Pressure in the Cooling Process Based on a Multi-Model Fusion Neural Network

YUSEN GENG, XIAOHONG WANG, AND PING JIANG
School of Electrical Engineering, University of Jinan, Jinan 250022, China

Corresponding author: Ping Jiang (cse_jiangp@ujn.edu.cvan)

This work was supported in part by the National Natural Science Foundation of China under Grant 61601197, in part by the Natural Science Foundation of Shandong Province in China under Grant ZR2016FL07, and in part by the Shandong Province's Independent Intelligent Collaborative Control and Optimization Key Technology Research and Application Demonstration Project under Grant 2017CXGC0614.

ABSTRACT The reasonable control of the grate cooler is the key factor to ensure the heat exchange and cement clinker quality during the clinker cooling process. In this paper, the cement grate cooler pressure of the grate cooler is taken as the research object and a cement grate cooler pressure prediction model is proposed based on the analysis of the current status of the automatic control of the grate cooler. This model uses a multi-model fusion neural network algorithm that combines a BP neural network, a support vector machine and classification and regression trees with a neural network structure. Furthermore, the multi-model fusion quality characteristics are proposed, and the root mean square error and Pearson linear correlation coefficient of the multi-model fusion quality characteristics are used as the evaluation indicators for the prediction results of the multi-model fusion neural network. After the analysis of the cooling process of the cement clinker, we select seven input variables, and then complete the data preprocessing and model parameter selection. Finally, we predict the cement grate cooler pressure using a multi-model fusion neural network, a BP neural network, a support vector machine and classification and regression trees with three training sets to test sets ratios. Through the comparison of the root mean square error and the Pearson linear correlation coefficient evaluation indicators and their change trends, as well as the display and analysis of the final modelling results, it is found that the multi-model fusion neural network algorithm can greatly improve the accuracy of the prediction of the grate pressure, and at the same time it has good practicality for the accurate prediction of the cement grate cooler pressure in the industry.

INDEX TERMS The grate cooler pressure, multi-model fusion neural network, multi-model fusion quality characteristics.

I. INTRODUCTION

The cement cooling process is an essential process in cement production. The stability of this process will directly determine the quality of the produced cement and the heat exchange efficiency. Because the cement cooling process has nonlinearity, strong coupling, a large time lag and other characteristics, it is essential to control the cement cooling process. The cement cooling process technology is shown as follows in Fig.1.

The cement grate cooler is the main equipment of the cement cooling process. As process equipment, it undertakes the task of cooling the high temperature clinker and crushing it to meet the requirements of clinker transportation, storage and cement grinding. At the same time as cooling the clinker, the thermal equipment undertakes the task of heating

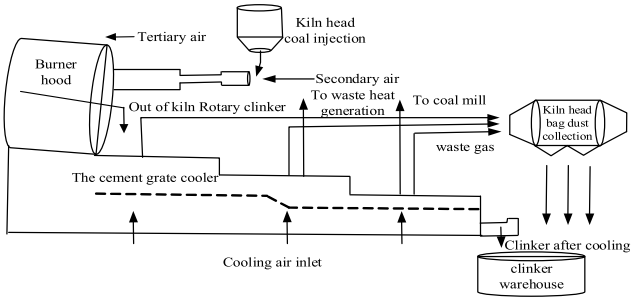

FIGURE 1. The cement cooling process diagram.

The associate editor coordinating the review of this manuscript and approving it for publication was Sotirios Goudos.

the secondary air that enters the rotary kiln and the tertiary air that enters the decomposing furnace. The heat recovery equipment undertakes the task of recovering a large amount of waste heat from the kiln clinker, which is used for waste heat power generation and coal mill drying. In addition, the clinker conveying device undertakes the task of conveying the high temperature clinker. Keeping the cement grate cooler pressure within a certain range is a prerequisite for the normal operations of the cement cooling process. Due to the four generations of grate coolers used in most modern cement production lines, the cooling fan speed is generally maintained at a relatively stable state. The cooling air device speed is adjusted only under special conditions, and so the air to volume ratio of the cooling air is rarely adjusted at the industrial site. Therefore, the cement cooling process usually maintains the cement grate cooler pressure by adjusting the idle speed of the grate cooler. When the cement grate cooler pressure is too high, the material layer of the rotary kiln clinker is thicker, and the cooling air device cannot easily blow through the material layer. At this time, the secondary air temperature of the air that enters the rotary kiln, the tertiary air temperature of the air that enters the decomposing furnace and the electric hot air temperature of the air that enters the waste heat power generation system are higher, and the energy utilization rate is improved; however, the clinker cooling effect is not good, and the energy utilization rate is increased at the cost of the cooling effect. In addition, the thickness of the clinker layer entering the grate cooler is thin. Although the cooling effect of the clinker is guaranteed, the secondary air temperature and the tertiary air temperature cannot meet the requirements, which will directly affect the pre-decomposition effect of the cement raw material and the stable operations of the burning process. Hence, keeping the cement grate cooler pressure within a certain range can definitely guarantee the normal operations of the cement cooling process.

Combined with the cement cooling process technology, it can be seen that the cement grate cooler has an important role in the cement production process. It is the key equipment for heat exchange and guaranteeing the quality of the cement clinker in the production process. However, fewer control points for the cement grate cooler in a domestic cement factory results in difficulties modelling the cement grate cooler. The cement grate cooler is still controlled manually, and so the cement grate cooler is controlled by the control short board in the cement production process. Aiming at the current situation of cement grate cooler control, a parameter prediction model of the cement grate cooler is proposed to achieve the automatic control of the whole cement production process and save energy and reduce the costs of cement enterprises [1].

After reading the relevant documents, it is found that much research, domestic and foreign, has been done on the control and optimization settings of the cement cooling process. For example, Hu [2], set up a cement grate cooler pressure optimal setting model based on cement technology to realize the optimal control for cement grate cooler optimization. The model consists of the cement grate cooler pressure presetting model based on an LS-SVM and the cement grate cooler pressure setting correction model based on a Fuzzy system. Kang [3] used the improved BP neural network algorithm to establish the control model of the cement grate cooler system and proposed a new control algorithm. After reading a large number of documents, it is found that scholars usually use multiple algorithms to build models, then make a comprehensive comparison of the results, and finally select the best algorithms for predictive modelling. However, this method cannot overcome the problem that the prediction model parameters are not fixed, many experiments are needed to select the best model parameters for Predictive modelling, the parameter adjustment process is cumbersome and the modelling takes a long time; therefore, the actual application effect is not good. In response to these problems, some scholars have overcome the problems by adding optimization algorithms in the model building process For example, Zhang [4] used an IGA-MK LS-SVM algorithm and an adaptive multi-group NSGA-II genetic algorithm to model and optimize the key parameters of a cement grate cooler. Kumar *et al.* [5] used the modified entropy yields caused by heat transfer and viscous dissipation as the objective functions, and used a genetic algorithm to optimize the multi-objective parameters of the cement grate cooler to improve the heat transfer efficiency. After adding the optimization algorithm, the accuracy of the parameter selection of the model algorithm is improved and the prediction error is reduced. However, the whole process needs to encode and decode the problem, and most of the parameters of the optimization algorithm still depend on experience, which will affect the model prediction results.

To conquer the above problems, this paper proposed a new prediction method for the cement grate cooler pressure in the cooling process. In this paper, the root mean square error (*RMSE*) and the Pearson Linear Correlation Coefficient (*PLCC*) are used as the comparative evaluation indexes of the model prediction quality and the multi-model fusion quality characteristics (MFQCs),and a multi-model fusion neural network are proposed. Based on a large number of experiments, the BP neural network (BP), the support vector machine (SVM) and Classification and Regression Trees (CART) [6], which are commonly used in cement industry prediction model modelling, are selected and fused into an algorithm. Next, the fused algorithm is used in the prediction model of the cement grate cooler pressure in the cement production cooling process, which provides the parameter target for realizing the automatic control of the grate cooler.

II. PROCESS MECHANISM ANALYSIS AND SELECTION OF MODELLING VARIABLES

A. GRATE COOLER PROCESS MECHANISM ANALYSIS

1) MECHANISM ANALYSIS OF THE HEAT BALANCE PROCESS OF A GRATE COOLER

The selection of the modelling variables has an inseparable relationship with the prediction accuracy of predictive

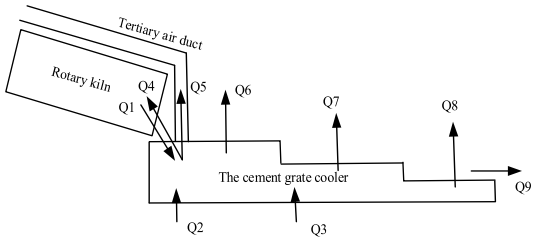

FIGURE 2. Heat balance process mechanism of the cement grate cooler.

TABLE 1. Table of the cement grate cooler heat balance parameters.

Symbol	Parameter	Dimension
Q1	Sensible heat in the cement grate cooler Clinker	KJ/Kg
Q2	Sensible heat in the cement grate cooler air	KJ/Kg
Q3	Sensible heat leaking into the cement grate cooler	KJ/Kg
Q4	Secondary air sensible heat	KJ/Kg
Q5	Tertiary air sensible heat	KJ/Kg
Q6	Residual air sensible heat of the cement grate cooler	KJ/Kg
Q7	Sensible heat in the AQC furnace air	KJ/Kg
Q8	The drying air sensible heat of the mill	KJ/Kg
Q9	Sensible heat out of the cement grate cooler Clinker	KJ/Kg

models. Since the cement industry is a typical process industry, the production process is closely related and coupled. The selection of the modelling variables cannot be limited to a single process. According to the heat balance process mechanism of the cement grate cooler, the burning process is closely related to the cooling process. The heat balance process of the cement grate cooler is shown as follows in Fig.2.

According to the parameters in table 1, the heat balance formula of the grate cooler can be obtained [7]:

$$Q1 + Q2 + Q3 = Q4 + Q5 + Q6 + Q7 + Q8 + Q9 \quad (1)$$

The heat balance of the grate cooler is a steady-state balance, which determines the heat exchange efficiency between the grate cooler and the rotary kiln. It has a certain influence on the temperature of the rotary kiln and the grate cooler pressure of the cement grate cooler. In the production of the cement industry, when no special working conditions occur, the operator usually controls the rotary kiln and grate cooler according to this equation so that the temperature of the rotary kiln and the grate cooler pressure are stabilized within a reasonable range, and then the production process is stabilized. According to the mechanism of the heat balance process of the cement grate cooler, it is found that the influencing factors of the grate cooler pressure are closely related to the burning process and cooling process. Therefore, the variables required for the modelling of the grate cooler prediction model need to be selected from the burning and cooling sections.

2) ANALYSIS OF THE EFFECT OF THE ROTARY KILN ON THE COOLING EFFECT OF THE GRATE COOLER

The calcination of the clinker is mainly done by the rotary kiln. The formation of high-quality clinker is closely related to the rotary kiln. The formation of high-quality clinker must maintain a certain high temperature in the rotary kiln and ensure that the material stays in the rotary kiln for a set amount of time. When the temperature of the firing zone in the rotary kiln is suitable and the residence time of the clinker is reasonable, the granules of the clinker in the rotary kiln are uniform and the temperature is suitable. At this time, by reasonably controlling the grate down pressure, a better cooling effect can be ensured. When the rotary kiln temperature is too high, it is difficult to ensure a uniform clinker particle size, which results in caking of the rotary kiln clinker, blocking of the grate holes, and the special ''snowman'' condition, which affects the cooling effect.

3) ANALYSIS OF THE EFFECT OF THE GRATE COOLER COOLING EFFECT ON THE ROTARY KILN TEMPERATURE

The cold air blown by the cooling fan penetrates the high-temperature clinker to cool the clinker and generate secondary air. The main function of the secondary air is to enter the rotary kiln to provide enough heat for the rotary kiln. The secondary air can affect the combustion state of the flame in the kiln, which affects the temperature change of the burning zone of the rotary kiln; and the rational use of secondary air can reduce coal consumption and reduce energy waste. The temperature of the secondary air not only reflects the heat exchange effect between the high-temperature clinker and the cooling air but also reflects how much heat the rotary kiln receives from the grate cooler.

When the secondary air temperature is too high, the heat exchange efficiency between the rotary kiln and the grate cooler is high, the flame of the coal injection pipe of the kiln head is shortened and drifts upward, and the combustion of pulverized coal accelerates, which will cause local high temperatures and easily damage the kiln skin and refractory brick. This affects the safe operation of the rotary kiln. When the secondary air temperature is low, the heat exchange efficiency between the rotary kiln and the grate cooler is low. At this time, the black fire head of the kiln head coal injection pipe is longer, the flame becomes longer, and the heat is dispersed. The calcination in the rotary kiln occurs at a lower temperature.

B. SELECTION OF MODELLING VARIABLES

To ensure the effect of the related functions of the clinker cooling process, the working state of the grate cooler needs to be monitored. Through the above analysis of the related processes of the grate cooler, it is found that the grate cooler

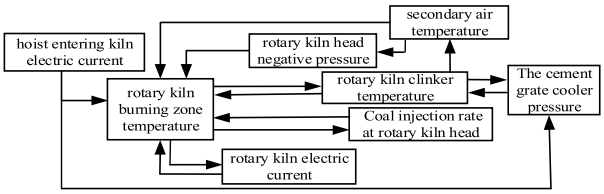

FIGURE 3. The modelling variables relationship diagram.

is closely related to the production process of the rotary kiln. Through the coordinated control of the grate cooler and the rotary kiln, the clinker can be quickly cooled during the cement cooling process, and the thermal efficiency of the grate cooler can be improved, which improves the quality of the clinker. Therefore, the working state parameters of the grate cooler and the rotary kiln need to be set. This part involves many parameters, but many parameters are not used as the basis for regulation in the industrial site. When the operating conditions of the grate cooler and the rotary kiln change, the operator of the central control room often makes judgements and adjustments based on several fixed parameters. According to the above analysis of the grate cooler related process and the summary of an excellent operator's operating experience in the central control room, the following 8 process parameters are selected as the main modelling variables, and these 8 main modelling variables are used as the input variables for the grate pressure prediction model. The relationship diagram of the model input variables is shown in Fig.3.

The graph in Figure 3 illustrates the closed-loop relationship between the partial modelling variables and the cement grate cooler pressure. Due to the complex mechanism and strong coupling of the burning and cooling process, the specific mathematical functional relationship cannot be found between the modelling variables in the actual production process. The approximate relationship between the modelling variables is as follows.

The hoist entering kiln electric current reflects the amount of raw material in the rotary kiln during a period of time. As the amount of raw material that enters the rotary kiln increased, the hoist entering kiln electric current becomes larger. Because of the evaporation of water during the drying process of the raw meal, water vapour is formed and carbon dioxide is released. Therefore, the temperature of the exhaust gas in the rotary kiln first decreases. When the raw material reaches the burning zone in the rotary kiln, the rotary kiln burning zone temperature is decreased, the amount of clinker from the rotary kiln is increased, and the cement grate cooler pressure becomes larger.

When the cement grate cooler pressure is too high, the rotary kiln clinker layer is too thick for the cooling air to blow through the material layer, which leads to the rise of the secondary air temperature. The increase of the secondary air temperature adversely affects the temperature of the rotary kiln burning zone, and then it changes the amount of injected coal.

When the amount of injected coal increases, in the oxidation stage, the temperature of the rotary kiln burning zone increases, and the temperature of the clinker out of the rotary kiln increases. At this time, the idle speed of the cement grate cooler increases, the heat dissipation accelerates, and the pressure of the cement grate cooler decreases. When overburning, the combustion enters the reduction phase, the air in the rotary kiln is consumed and the carbon dioxide increases, Then, the temperature of the rotary kiln is reduced the temperature of the clinker in the rotary kiln is lowered, the idle speed of the grate cooler is reduced, and the cement grate cooler pressure is increased.

The changes in the rotary kiln electric current reflect the burning conditions in the rotary kiln. When the amount of raw material entering the rotary kiln increases or the temperature of the rotary kiln burning zone increases, the minerals added to the liquid phase increase and the viscosity also increases, which will cause the load to increase when the rotary kiln rotates and the rotary kiln electric current becomes larger. In both cases, the cement grate cooler pressure will be changed, and so the rotary kiln electric current is also an indirect indicator of the cement grate cooler pressure. When the idle speed of the grate cooler is too fast, the clinker comes out of the cement grate cooler without being completely cooled. At this time, the secondary air temperature and the temperature before the rotary kiln are reduced, and the pulverized coal cannot be burned as soon as possible; therefore, the rotary kiln burning zone temperature decreases and the rotary kiln electric current drops.

The rotary kiln head negative pressure is a reaction indicator of the balance of the air volume in the cement cooling process. It mainly includes the volumes of the cooling air, the secondary air, the tertiary air and the residual air of the grate cooler, which can indirectly reflect the underarm pressure during this period.

III. DATA PREPROCESSING

This paper take a 5000 t/d production line in a cement factory in Shandong Province as its background, and this model is only suitable for the automatic control of the grate cooler pressure when no special working conditions occur. Our collection of modelling data uses the OLE for Process Control (OPC) protocol to read the on-site production data from the distributed computer system (DCS) to the on-site database. Then, we extract the data on continuous and stable production from the on-site database and send them to a local computer for grate cooler pressure prediction model modelling. Considering the data have large fluctuations andinstability, if the amount of data is too large, the speed of the analysis will become slower; conversely, less data are not enough to prove the correctness of the analysis. Therefore, the data extracted in the field are first subjected to data preprocessing in order to reduce the modelling effect caused by the data.

TABLE 2. Leyte criteria data sample.

Technological indexes	Average	Standard deviation
The cement grate cooler pressure (Pa)	7550.34	231.14
Rotary kiln burning zone temperature (°C)	1409.23	29.60
Rotary kiln clinker temperature (°C)	1278.95	19.97
Coal injection rate at rotary kiln head (t/h)	11.73	0.23
Rotary kiln head negative pressure (Pa)	-77.37	13.70
Rotary kiln electric current (A)	888.65	49.68
Hoist entering kiln electric current (A)	237.54	3.29
Secondary air temperature (°C)	1181.38	15.02

A. ELIMINATION OF LARGE DEVIATION DATA BASED ON LEYTE CRITERION

We use the following equation to find the mean value of the field data of the modelling variables:

$$\overline{x} = \sum_{i=1}^{n} x_i \tag{2}$$

We find the data deviation V_i as follows:

$$V_i = x_i - \overline{x} \tag{3}$$

We calculate the standard deviation of the modelling variables and the target vectors σ as followsčž

$$\sigma = \sqrt{\frac{\sum_{i=1}^{n} V_i^2}{n-1}} \tag{4}$$

If the absolute value of the deviation is greater than three standard deviations, which is $|V_i| > 3\sigma$, it is considered that x_i is abnormal datum and should be excluded. The averages and standard deviations are shown in Table 2.

B. ELIMINATION OF ABNORMAL DATA BASED ON THE PROCESS INDEX AND FIELD PRODUCTION INDEX

After the elimination of data with large deviations, we need to avoid the impact of data with large deviations on the modelling predictive models. Due to the differences in the main components of the raw materials for cement production, the automation level of the production equipment, the age of the production equipment and the operating experience of the field operators, many production parameters will fluctuate, and process parameters will also fluctuate; however, the process parameters fluctuate less and the production parameters will fluctuate more due to different advanced levels of production equipment. Table 3 shows the specifications of the process parameters related to the 5000 t/d production line under normal conditions.

According to the fluctuation range of the technological indexes during the long-term stable operations of the on-site production line, combined with the process indexes in Table 3, the comprehensive indexes suitable for the relevant process parameters of the production line are given again, as shown in Table 4.

TABLE 3. Technological indexes and reference indicators.

Technological indexes	Adjusted standard value
The cement grate cooler pressure	Approximately 5000 Pa
Rotary kiln burning zone temperature	1350°C-1450°C
Rotary kiln clinker temperature	1200°C-1350°C
Coal injection rate at rotary kiln head	10 t/h -15 t/h
Rotary kiln head negative pressure	20-50 Pa
Rotary kiln electric current	400-700 A
Secondary air temperature	1100°C-1250°C

TABLE 4. Technological indexes and comprehensive indicators.

Technological indexes	Adjusted standard value
The cement grate cooler pressure	7000 -8000 Pa
Rotary kiln burning zone temperature	1350°C-1450°C
Rotary kiln clinker temperature	1200°C-1350°C
Coal injection rate at rotary kiln head	10 t/h -15 t/h
Rotary kiln head negative pressure	50-90 Pa
Rotary kiln electric current	700-1050 A
Secondary air temperature	1100°C-1250°C

According to the comprehensive indicators, the collected production data have been standardized, and some unqualified indicators have been eliminated. Finally, the remaining 5118 sets of data are used as the experimental data in this paper.

C. DATA NORMALIZATION

Different modelling variables have different dimensions and dimensional units. This situation will affect the data analysis results. To eliminate the dimensional influence between modelling variables, data standardization needs to be performed. This paper normalizes the modelling variables after data normalization, and normalizes the modelling variables to 0-1 so that the indicators are on the same order of magnitude, which is suitable for the comprehensive comparative evaluation. The normalization formula is as follows:

$$X_i = \frac{x_i - \min(x)}{\max(x) - \min(x)} \tag{5}$$

Here, $X_i\,(1 \le X_i \le 5118)$ is the number of modelling variables; $\max(x)$ and $\min(x)$ are the maximum and minimum values of the modelling variables, respectively; and $X_i\,(1 \le X_i \le 5118)$ is normalized data. After three data processing steps, the modelling variables are shown in Fig.4.

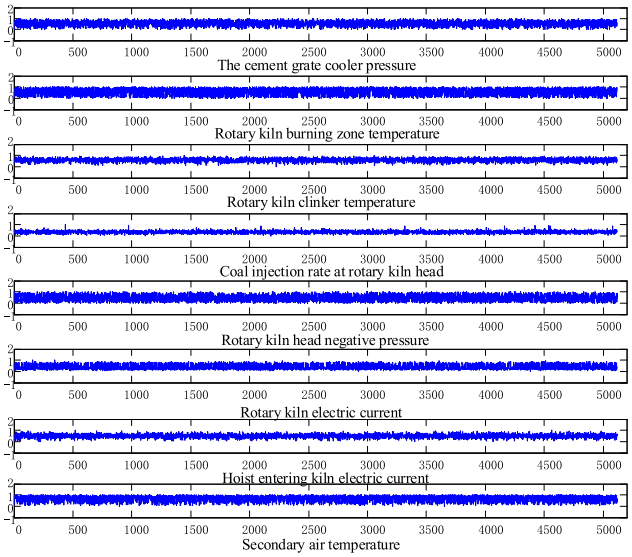

FIGURE 4. Modelling variables are normalized to 0-1.

IV. QUALITY EVALUATION METHOD OF THE FUSION MODEL BASED ON THE MFQCs

A. PROPOSED QUALITY EVALUATION METHOD FOR A FUSION MODEL BASED ON THE MFQCs

At present, the prediction of the cement grate cooler pressure is mostly conducted using a single model. Different models have different abilities to express data, and so the predicted results are also inconsistent. For example, an SVM uses an inner product kernel function instead of nonlinear mapping to a high-dimensional space. The final result is determined by a small number of vectors, which can capture the main samples; however, the SVM itself has a drawback that it is difficult to implement for large data sets. A BP neural network can conduct large-scale data set training, it can perform nonlinear mapping, and it has a strong generalization ability. However, when using the gradient descent method, the convergence speed is slow, and it is easy to fall into the local optimum value, resulting in training failure. The prediction effect evaluation for a single model can be compared with the original data using a single model prediction, and it can be used to evaluate the quality of the model prediction [8].

In this paper, a variety of algorithms are used to form a fusion model. The results of a single model prediction cannot evaluate the prediction effect of the fusion model. According to analysis the characteristics of the proposed model fusion algorithm, the results predicted by a single algorithm are fused, and the fusion results are compared with the original data. Then, its *RMSE* or *PLCC* is calculated to evaluate the quality of the model prediction. To facilitate the recording and evaluation, the results of the fusion of the single algorithm prediction results are named the multi-model fusion quality characteristics, and the quality of the fusion model is evaluated by using the *RMSE* and *PLCC* of the multi-model fusion data quality features.

B. DESIGN MFQCs

The formation of the MFQCs mainly adopts a combination strategy. As shown in formula (6), $f_i(x)$ models node i, and W_i is the weight corresponding to the model [9].

$$F(x) = \sum_{i=1}^{m} W_i f(x) \tag{6}$$

The weights are obtained in two ways: the *PLCC* and the *RMSE*.

1) Use the *RMSE* to get the weight. *RMSE* is the root mean square error, and its calculation formula is shown in formula (7). The smaller the value is, the higher the prediction quality of the model and the higher the accuracy of the algorithm. is the raw data and is the forecasted data.

$$RMSE = \left[\frac{1}{n}\sum_{i=1}^{n}(x_i - y_i)^2\right]^{\frac{1}{2}} \tag{7}$$

The weight calculation formula is shown in formula (8). $RMSE_i$ is the *RMSE* value of node i's model prediction data.

$$\begin{cases} W_i = \dfrac{RMSE_i^{-1}}{\sum\limits_{j=1}^{n} RMSE_i^{-1}} \\ F(x) = \sum\limits_{i=1}^{m} W_i f_i(x) \end{cases} \tag{8}$$

2) Use the *PLCC* to get the weight. *PLCC* is the Pearson coefficient and is an indicator of the linear correlation between two results. The higher the value is, the higher the linear correlation. Its calculation formula is as shown in formula (9), where x_i is the raw data and y_i is the forecasted data.

$$PLCC = \frac{1}{n-1}\sum_{i=1}^{n}\left(\frac{x_i - \bar{x}}{\sigma_x}\right)\left(\frac{y_i - \bar{y}}{\sigma_y}\right) \tag{9}$$

The weight calculation formula is shown in formula (10). $PLCC_i$ is the *PLCC* value of the model of node i's prediction data.

$$\begin{cases} W_i = \dfrac{PLCC_i}{\sum\limits_{j=1}^{n} PLCC_j} \\ F(x) = \sum\limits_{i=1}^{m} W_i f_i(x) \end{cases} \tag{10}$$

C. INTRODUCTION TO SCORING MODEL

After reading many documents, this paper decides to use the BP neural network algorithm (BP), the support vector machine algorithm (SVM) and the classification and regression trees algorithm (CART) to construct the predictive model of the underarm pressure.

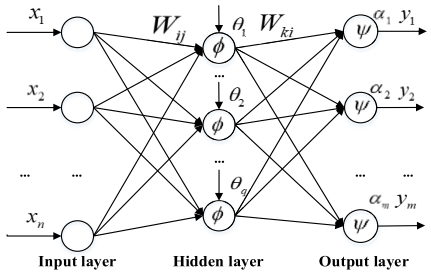

FIGURE 5. BP neural network structure.

1) NEURAL NETWORK MODEL

The BP neural network algorithm is the most widely used neural network algorithm. The algorithm has two major features: forward propagation of the input signal and backward correction of the weight threshold. The structure of the BP neural network is shown in Fig.5.

The input of the BP neural network is $x = [x_1 x_2 \cdots x_n]$ and the output is $y = [y_1 y_2 \cdots y_m]$. The weights between neurons are W_{ij} and W_{jk}, $\phi(x)$ is the implicit layer activation function, and $\psi(x)$ is the output layer activation function [10].

1) Forward propagation of signals
Input net_i of node i in the implicit layer:

$$net_i = \sum_{j=1}^{n} W_{ij} x_j + \theta_i \tag{11}$$

Output net_i of node i in the implicit layer:

$$y_i = \phi(net_i) = \phi\left(\sum_{j=1}^{n} W_{ij} x_j + \theta_i\right) \tag{12}$$

Input net_k of node k in the output layer:

$$\begin{aligned} net_k &= \sum_{i=1}^{q} W_{ki} + \alpha_k \\ &= \sum_{i=1}^{q} W_{ki} \phi\left(\sum_{j=1}^{n} W_{ij} x_j + \theta_i\right) + \alpha_k \end{aligned} \tag{13}$$

Output y_k of node k in the output layer:

$$\begin{aligned} y_k &= \psi(net_k) = \psi\left(\sum_{i=1}^{q} W_{ki} + \alpha_k\right) \\ &= \psi\left(\sum_{i=1}^{q} W_{ki} \phi\left(\sum_{j=1}^{n} W_{ij} x_j + \theta_i\right) + \alpha_k\right) \end{aligned} \tag{14}$$

2) Reverse correction of the of errors
The quadratic error criterion function for each sample p is E_p:

$$E_p = \frac{1}{2} \sum_{k=1}^{m} (T_k - y_k)^2 \tag{15}$$

The total error criterion function of the system for training samples with the number p is as follows:

$$E = \frac{1}{2} \sum_{1}^{p} \sum_{k=1}^{m} \left(T_k^p - y_k^p\right)^2 \tag{16}$$

According to the error gradient descent method, the correction amount ΔW_{ki} of the output layer weight value, the correction amount $\Delta\alpha_k$ of the output layer threshold value, the correction amount ΔW_{ij} of the implicit layer weight value and the correction amount $\Delta\theta_i$ of the implicit layer threshold value are sequentially corrected.

$$\begin{aligned} \Delta W_{ki} &= -\eta \frac{\partial E}{\partial W_{ki}}; \quad \Delta\alpha_k = -\eta \frac{\partial E}{\partial \alpha_k} \\ \Delta W_{ij} &= -\eta \frac{\partial E}{\partial W_{ij}}; \quad \Delta\theta_i = -\eta \frac{\partial E}{\partial \theta_i} \end{aligned} \tag{17}$$

Output layer weight value adjustment formula:

$$\begin{aligned} \Delta W_{ki} &= -\eta \frac{\partial E}{\partial y_k} \frac{\partial y_k}{\partial net_k} \frac{\partial net_k}{\partial W_{ki}} \\ &= \eta \sum_{p=1}^{p} \sum_{k=1}^{m} \left(T_k^p - y_k^p\right) \cdot \psi'(net_k) \cdot y_i \end{aligned} \tag{18}$$

Output layer threshold adjustment formula:

$$\begin{aligned} \Delta\alpha_k &= -\eta \frac{\partial E}{\partial y_k} \frac{\partial y_k}{\partial net_k} \frac{\partial net_k}{\partial \alpha_k} \\ &= \eta \sum_{p=1}^{p} \sum_{k=1}^{m} \left(T_k^p - y_k^p\right) \cdot \psi'(net_k) \end{aligned} \tag{19}$$

Implicit layer weight adjustment formula:

$$\begin{aligned} \Delta W_{ij} &= -\eta \frac{\partial E}{\partial y_i} \frac{\partial y_i}{\partial net_i} \frac{\partial net_i}{\partial W_{ij}} \\ &= \eta \sum_{p=1}^{p} \sum_{k=1}^{m} \left(T_k^p - y_k^p\right) \\ &\quad \cdot \psi'(net_k) \cdot W_{ki} \cdot \phi'(net_i) \cdot x_j \end{aligned} \tag{20}$$

Implicit layer threshold adjustment formula:

$$\begin{aligned} \Delta\theta_i &= -\eta \frac{\partial E}{\partial y_i} \frac{\partial y_i}{\partial net_i} \frac{\partial net_i}{\partial \theta_i} \\ &= \eta \sum_{p=1}^{p} \sum_{k=1}^{m} \left(T_k^p - y_k^p\right) \cdot \psi'(net_k) \cdot W_{ki} \cdot \phi'(net_i) \end{aligned} \tag{21}$$

2) SUPPORT VECTOR MACHINE MODEL

The core of a support vector machine is to find a non-linear function. Through this function, the given sample $D = \{(x_1, y_1), (x_2, y_2), \ldots, (x_m, y_m)\}$ is mapped from a low-dimensional space to high-dimensional space F, the original non-linear problem is converted into a linear problem, and the following regression model formula is obtained:

$$f(x) = \omega^T x + b \tag{22}$$

ω is the weight vector of space F; and b is the intercept, which determines the position of the hyperplane.

The SVM problem is formalized as formula (23):

$$\min_{\omega,b,e} J(\omega, e) = \frac{1}{2}\omega^T\omega + \frac{1}{2}C\sum_{i=1}^{N} e_i^2$$
$$s.t. y_i = w^T x + b + e_i \quad i = 1, 2, \ldots, N \tag{23}$$

where e_i is the error variable and C is the penalty factor, which represents the tolerance for errors. The larger C is, the smaller the tolerance for errors, and the easier it is for the model to be overfit. The smaller C is, the easier it is for the model to be underfit. If C is too large or too small, the generalization ability of the model will deteriorate. In the SVM program, C is represented by gamma.

The conditional problem under the priority constraint is transformed into an unconstrained optimization problem by Lagrange function, and the output after grouping according to the radial basis function is expressed as formula (24).

$$y = f(x) = \sum_{i=1}^{N} \lambda_i \cdot \exp\left(-\frac{(x - x_i)^2}{2 \cdot \sigma^2}\right) + b \tag{24}$$

Among them, the input quantity is x, the output quantity is y, λ_i is the Lagrange multiplier, and σ^2 is a parameter of the kernel function [11].

3) CLASSIFICATION AND REGRESSION TREES

The overall flow of the regression tree is similar to the classification tree. When branching, it exhausts every threshold of every feature to find the optimal segmentation feature j and the optimal segmentation point. The goal is to minimize the squared error. Branches do not stop until a preset termination condition (such as the upper limit of the number of leaves) is reached [12].

Using the minimum squared difference criterion, the input of the training data set is

$$D = \left\{\left(x_1, y_1\right), \left(x_2, y_2\right), \ldots, \left(x_m, y_m\right)\right\} \tag{25}$$
$$\min_{j,s}\left[\min_{c_1}\sum_{x_i \in R_1(j,s)}(y_i - c_1)^2 + \min_{c_2}\sum_{x_i \in R_2(j,s)}(y_i - c_2)^2\right]$$
$$\hat{c}_m = \frac{1}{N_m}\sum_{x_i \in R_2(j,s)} y_i \quad x \in R_m, m \in 1, 2 \tag{26}$$

where c_1 and c_2 are the average output values in intervals R_1 and R_2, respectively. To minimize the squared error, we need to traverse each value of each feature in turn, calculate the error of each possible segmentation point at present, then select the point with the smallest segmentation error to divide the input space into two parts, and finally recursively perform the above steps until the segmentation is finished to form the regression tree $f(x)$ [13].

$$f(x) = \sum_{m=1}^{M} c_m I(x \in R) \tag{27}$$

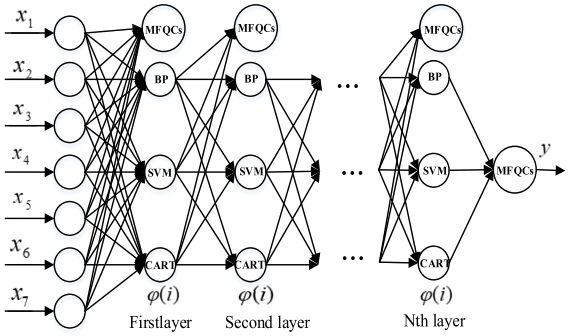

FIGURE 6. Multi-model fusion neural network structure.

V. MULTI-MODEL FUSION NEURAL NETWORK

The multi-model fusion neural network is an evolution of the traditional neural network, and it has the structure of a neural network. The 1-n middle layer of the multi-model fusion neural network is similar to the hidden layer of the traditional neural network. The middle layer neurons of the multi-model fusion neural network are a single BP neural network, an SVM and CART. The structure of the Multi-model fusion neural network is shown in Fig.6 [14]. While the traditional neural network models are signal forward propagation and error back propagation, the multi-model fusion neural networks only have signal forward propagation, and the error back propagation is adjusted in the middle layer neurons.

The multi-model fusion neural network's input is $x = [x_1 x_2 x_3 x_4 x_5 x_6 x_7]^T$, the output is y, the weight between neurons is 1, $\phi(i)$ is the middle layer algorithm, the BP algorithm is named 1, the SVM algorithm is named 2 and the CART algorithm is named 3.

The input of the middle layer neuron is net_i $(i = 1, 2, 3)$.

The output of the middle layer neurons is y_i:

$$y_i = \phi(net_i) \tag{28}$$

The outputs of the three neurons in the middle layer of the first layer are y_1, y_2 and y_3, respectively. The MFQCs feature combination is performed according to the *RMSE* indicators, and the output is y:

$$y = y_i \frac{RMSE_i^{-1}}{\sum_{i=1}^{3} RMSE_i^{-1}} \tag{29}$$

The MFQC feature combination is performed according to the *PLCC* indicators, and the output is y:

$$y = y_i \frac{PLCC_i}{\sum_{i=1}^{3} PLCC_i} \tag{30}$$

VI. EXPERIMENTAL DESIGN AND RESULTS ANALYSIS

A. MODELLING PARAMETER SELECTION

Because the weight of each algorithm neuron in each middle layer of the multi-model fusion neural network is 1, the parameter selection of the entire fusion model is divided

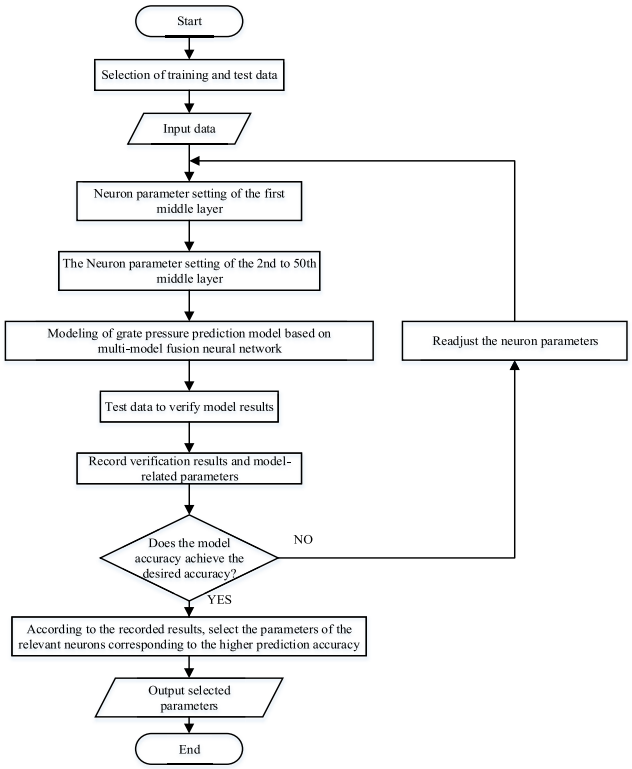

FIGURE 7. Model parameter selection process.

into two parts: the selection of the algorithm neuron parameters for each middle layer and the selection of the number of middle layers.

1) THE SELECTION OF THE ALGORITHM NEURON PARAMETERS FOR EACH MIDDLE LAYER

As seen from Fig.6, the number of input variables of each algorithm neuron in the first middle layer and the 2-n middle layer is different, and so the process needs to be divided into two parts to select the relevant parameters.

The main characteristics of the traditional BP neural network are the forward propagation of the input signal and the reverse correction of the errors. We use the ideas of the traditional BP neural network signal forward propagation and error direction correction to select the algorithm neuron parameters of each middle layer by trial and error. The process of selecting the algorithm neuron parameters of each intermediate layer through trial and error is shown in Fig.7.

Usually, there is not a fixed formula and method to find the number of neurons in the hidden layer of the neural network. To ensure the accuracy of the modelling results and prevent the occurrence of overfitting, in most cases, we usually set the number of initial hidden layer neurons to $2n + 1$ based on the number of input variables, and then we use a trial and error method to adjust it to an ideal state. $2n + 1$ is the number of hidden layers in a single BP neural network neuron. For a multi-model fusion neural network, the number of BP neuron input variables in the first middle layer and the second to Nth middle layers is different, and so the number of BP hidden layer neurons in the first middle layer is different from that of the second to Nth middle layers.

TABLE 5. Parameters of the neurons of the first middle layer.

Algorithm Neuron	Parameter Name	Numerical Value of 6:4	Numerical Value of 7:3	Numerical Value of 8:2
BP	Activation function	Sigmoid	Sigmoid	Sigmoid
	Maximum Number of Epochs	900	900	900
	Momentum Constant	0.7	0.8	0.95
	Learning Rate	0.05	0.05	0.05
	Minimum Gradient	1e-6	1e-6	1e-6
	Maximum Number of Validation Checks	5	5	5
	Number of hidden neurons	15	15	15
SVM	Transfer function	Radial Basis Function (RBF)	Radial Basis Function (RBF)	Radial Basis Function (RBF)
	Penalty factor (gam)	12	15	18
	Bandwidth in the case of the 'RBF_kernel' (sig2)	0.4	0.6	0.8
CART	Leaf node spacing	3	5	8
	The node that contains the minimum number of samples	(1,25)	(1,25)	(1,25)

After adjusting the number of BP hidden layer neurons using the trial and error method and then modelling it many times, it is found that the number of BP hidden layer neurons has little influence on the modelling results of the multi-model fusion neural network. Therefore, in order to simplify the complexity of the parameter selection in the modelling process without affecting the modelling results, we uniformly set the number of BP hidden layer neurons as $2n + 1$.

According to the above process, the relevant parameters of the model are finally determined as shown in Tables 5 and 6.

2) THE SELECTION OF THE NUMBER OF MIDDLE LAYERS

Through the adjustment of the middle layer of the multi-model fusion neural network, the prediction model of

TABLE 6. Parameters of the neurons of the 2nd to 50th middle layers.

Algorithm Neuron	Parameter Name	Numerical Value of 6:4	Numerical Value of 7:3	Numerical Value of 8:2
BP	Activation function	Sigmoid	Sigmoid	Sigmoid
	Maximum Number of Epochs	900	900	900
	Momentum Constant	0.65	0.73	0.88
	Learning Rate	0.05	0.05	0.05
SVM	Minimum Gradient	1e-3	1e-3	1e-3
	Maximum Number of Validation Checks	5	5	5
	Number of hidden neurons	7	7	7
	Transfer functions	Radial Basis Function (RBF)	Radial Basis Function (RBF)	Radial Basis Function (RBF)
	Penalty factor (gam)	10	14	16
	Bandwidth in the case of the 'RBF_kernel' (sig2)	0.4	0.6	0.8
CART	Leaf node spacing	3	5	8
	The node that contains the minimum number of samples	(1,20)	(1,20)	(1,20)

the cement grate cooler pressure is repeatedly modelled. The modelling results are shown in Table 7.

According to the comparison of the data in Table 7, regarding the accuracy of the model, when the number of middle layers is 30, the model accuracy is low; when the number of middle layers is 40, the accuracy increases; and after 50 layers, the accuracy tends to be gentle. Considering the running time of the model, as the number of intermediate layers increases, the running time of the model gradually increases. Combining the two factors of model accuracy and model running time, using 50 intermediate layers can obtain higher efficiency, and so the number of intermediate layers is fixed at 50 [15].

B. EXPERIMENTAL DESIGN

As being verified in the third chapter, as the evaluation indexes of the prediction model, the results proved that the

TABLE 7. Comparison of the modelling results for different numbers of middle layers.

The number of middle layer	Ratio of training to test data	computation time	RMSE of MFQCs	PLCC of MFQCs
30	6: 4	335s	0.1488	0.7649
	7: 3	346s	0.1436	0.7786
	8: 2	374s	0.1455	0.7781
40	6: 4	462s	0.1473	0.7737
	7: 3	498s	0.1456	0.7828
	8: 2	467s	0.1426	0.7963
50	6: 4	512s	0.1386	0.8073
	7: 3	535s	0.1357	0.8173
	8: 2	547s	0.1302	0.8344
60	6: 4	694s	0.1308	0.8284
	7: 3	702s	0.1315	0.8302
	8: 2	721s	0.1294	0.8510
70	6: 4	819s	0.1305	0.8217
	7: 3	835s	0.1285	0.8295
	8: 2	845s	0.1298	0.8532

RMSE and *PLCC* of the MFQCs are better than those of a single algorithm. Therefore, the multi-model fusion neural network after fusion uses the *RMSE* and *PLCC* of the MFQCs as the evaluation indexes of the model's prediction effect. After selecting the structure of the fusion model, this paper verified the prediction ability of the fusion model. The specific steps are as follows [16]:

1) Select 5118 data sets after data processing, and randomly separate the 5118 data sets into training sets and test sets at ratios of 6:4, 7:3, and 8:2;
2) Conduct proportional model modelling based on the BP neural network, the SVM, the CART and the multi-model fusion neural network;
3) Save the three proportional models established by the BP, SVM, and the CART and the multi-model fusion neural network, and then input the test data to test the models' accuracy;
4) Record the test results for the *RMSE*, the *PLCC* and the calculation time of the test results for the models established by BP, SVM, CART and multi-model fusion neural network;
5) Compare and analyse the *RMSE*, *PLCC*, and calculation time of the test results of the models established by the four algorithms; and
6) Display and analyse the change trends of the *RMSE* and *PLCC* of the middle layer MFQCs during the test process of the model established by the multi-model fusion neural network.

C. RESULT ANALYSIS

After experimental verification, all the results of the experiment are recorded, as shown in Table 8.

Table 8 shows the following.

TABLE 8. Fusion model prediction effect using verification data.

Ratio of training to test data	Prediction algorithm	computation time	RMSE	PLCC
6: 4	BP	10	0.1499	0.7687
	SVM	15	0.1496	0.7684
	CART	24	0.1510	0.7635
	Multi-model fusion neural network	508	0.1386	0.8073
7: 3	BP	12	0.1588	0.7388
	SVM	17	0.1523	0.7625
	CART	29	0.1516	0.7648
	Multi-model fusion neural network	527	0.1357	0.8173
8: 2	BP	15	0.1567	0.7486
	SVM	22	0.1556	0.7522
	CART	33	0.1529	0.7615
	Multi-model fusion neural network	539	0.1302	0.8344

1) According to the calculation time, the BP, SVM and CART are faster than the multi-model fusion neural network, but the accuracy of the BP, SVM and CART when predicting grate cooler pressure is much lower than that of the multi-model fusion neural network. After the analysis of the cement production process, the cement production process has the characteristics of a large time lag, and the grate cooler pressure does not need to be predicted in real time during production; therefore, for cement production, the prediction accuracy is much more important than the calculation time.
2) Under each training set to test set ratio, the differences among the prediction results of the cement grate cooler pressure prediction models established by the BP neural network, SVM and CART are not that much. Since the data are randomly selected, when a new set of data is extracted again, the prediction result will generate small-scale fluctuations, Due to the influence of these fluctuations, it is impossible to ensure which algorithm is more advantageous for predicting the cement grate cooler pressure.
3) Under the three ratios of the training set and test set, the underarm pressure predicted by the fusion model is significantly better than the model prediction results generated by the other three algorithms.

According to the results obtained in the above table, obviously, the fusion model prediction result is better than those of the single models. To further prove that the fusion model has better a prediction effect, the following is the trend graphs of the *RMSE* and *PLCC* changes of the middle layer MFQCs of the fusion model obtained through these three ratios. [17] In the figure, *RMSE*1 is the trend of the *RMSE* in the middle layer during the training of the model. *RMSE*2 is the trend of the *RMSE* in the middle layer during the fusion model test, and *PLCC*1 is the trend of the *PLCC* in the middle layer during the training of the model. *PLCC*2 is the trend of the *PLCC* in the middle layer during the fusion model test.

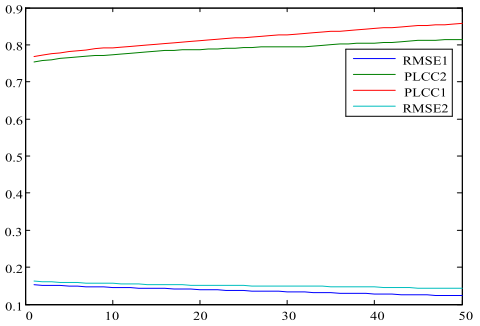

FIGURE 8. Trends of the *RMSE* and *PLCC* in the middle layer of the fusion model when the ratio of the training data to the test data is 6: 4.

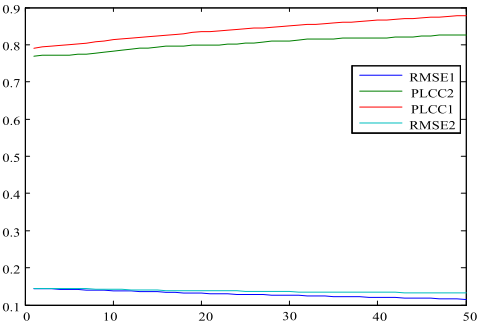

FIGURE 9. Trends of the *RMSE* and *PLCC* in the middle layer of the fusion model when the ratio of the training data to the test data is 7: 3.

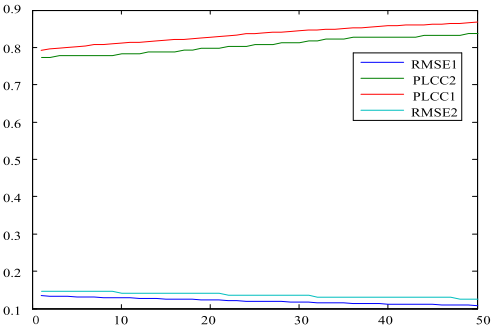

FIGURE 10. Trends of the *RMSE* and *PLCC* in the middle layer of the fusion model when the ratio of the training data to the test data is 8: 2.

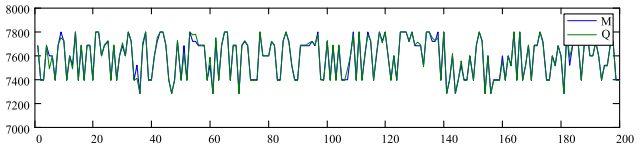

FIGURE 11. The actual prediction results and the first 200 groups of enlarged images when the ratio of training data to test data is 6: 4.

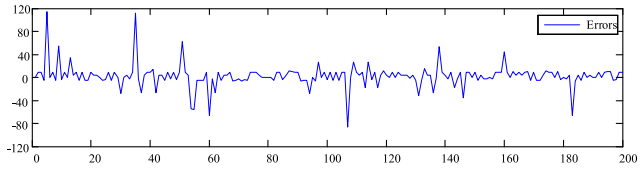

FIGURE 12. Actual forecasting error and the first 200 groups of enlarged pictures when the ratio of training data to test data is 6: 4.

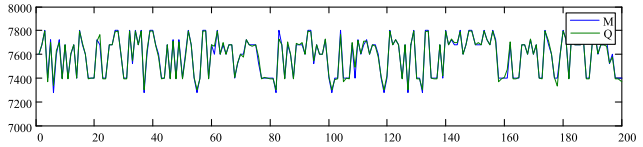

FIGURE 13. The actual prediction results and the first 200 groups of enlarged images when the ratio of training data to test data is 7:3.

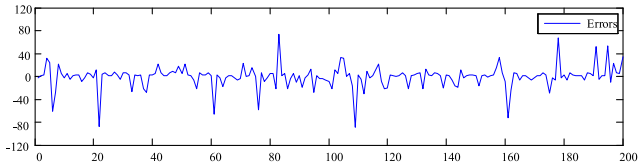

FIGURE 14. Actual forecasting error and the first 200 groups of enlarged pictures when the ratio of training data to test data is 7: 3.

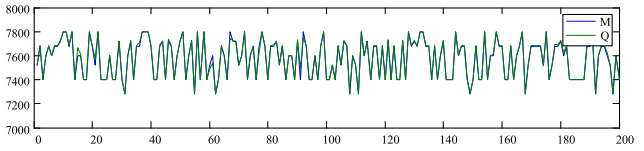

FIGURE 15. The actual prediction results and the first 200 groups of enlarged images when the ratio of training data to test data is 8: 2.

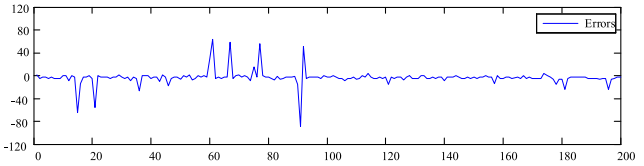

FIGURE 16. Actual forecasting error and the first 200 groups of enlarged pictures when the ratio of training data to test data is 8: 2.

The following can be derived from the above three figures.

1) At each ratio, the *RMSE* of the MFQCs of each middle layer gradually decreases, and the *PLCC* gradually increases. The smaller the *RMSE* is, the better the prediction effect. The larger the *RMSE* is, the better the prediction effect.
2) The larger the amount of data in the training set is, the more obvious the trend change, and the trends of the two indicators are more obvious than those in the test set.

Through the above experimental verification and comparison of the trend graphs, the accuracy of the cement grate cooler pressure prediction model established by the multi-model fusion neural network is higher than that of the cement grate cooler pressure prediction model established by a single algorithm.

Fig.11-16 show the actual prediction results. M represents the original test data set, and Q represents the prediction data of the grate cooler pressure using multi-model fusion neural network. Due to the large amount of prediction data, the specific prediction effect cannot be displayed well. To better judge the prediction effect, we enlarge the first 200 groups of the comparison results between the prediction data and the original data.

It can be seen from the error graph that the error fluctuation range of the predicted cement grate cooler pressure compared to the actual cement grate cooler pressure under the three ratios of training data to test data is Mostly within ±40Pa. Because there are many factors that affect the grate cooler pressure in industrial production, the grate cooler pressure is unstable. In industrial production, the grate cooler pressure fluctuates within a certain range, and the fluctuation range is about ±300Pa. Therefore, when the predicted result of the model is within ±300Pa of the actual value, it can truly reflect the actual situation of the grate cooler pressure and has no impact on the on-site regulation. Because the predicted results of the grate cooler pressure from the model based on the multi-model fusion neural network can be stabilized within ±120Pa of the actual value, the prediction results can reasonably reflect the actual cement grate cooler pressure and can provide a basis for the control of the cement grate cooler pressure on site.

VII. CONCLUSION

To improve the prediction of the cement grate cooler pressure, this paper proposed a method for predicting the cement grate cooler pressure based on information fusion. After recording and analysing the two experimental results, it is found that the fusion model can better predict the cement grate cooler pressure than a prediction model generated by a single algorithm. The prediction process of the fusion model is a process of continuously optimizing the prediction results of a single model. The greater the number of middle layers, the higher the prediction accuracy, and the more obvious the optimization effect. If the number of middle layers is set too high, the predictive model will run for a long time. Thus, this paper combined actual production with experiments. When the number of middle layers is below 50, the model prediction efficiency is high. The larger the amount of modelling data is, the better the prediction effect for the fusion model. Combined with the actual production on site, it is found that the cement cooling process will generate a large amount of production data, which meets the requirements for the modelling data of the fusion model. Therefore, the production data of the cement cooling process can be used for the fusion model's prediction of the cement grate cooler pressure. The prediction results produced by the information fusion method proposed in this paper are not accidental, which is why this paper intends to improve the accuracy by balancing the pre-

TABLE 9. English abbreviation definition.

Full name	Abbreviation
Back Propagation Neural Network	BP
Support Vector Machine	SVM
Classification and Regression Trees	CART
OLE for Process Control	OPC
Distributed computer system	DCS
Root Mean Square Error	RMSE
Pearson Linear Correlation Coefficient	PLCC
Multi-model Fusion Quality Characteristics	MFQCs

diction advantages of single algorithms through a reasonable design. This method is universal, it is easy to implement in engineering practice and it has broad practical prospects.

APPENDIX

See Table 9.

REFERENCES

[1] M. T. Sun, "Dynamic Bayesian network construction and prediction of pressure of state of cement grate cooler," M.S. thesis, School Inf. Sci. Eng., Yanshan Univ., Yanshan, China, 2018.
[2] G. W. Hu, "Research of cement grate cooler optimal control," M.S. thesis, School Automat. Elect. Eng., Jinan Univ., Jinan, China, 2013.
[3] X. Kang, "Research of control mode of cement grate cooler system," M.S. thesis, School Inf. Sci. Eng., Hebei Univ. Sci. Technol., Hebei, China, 2014.
[4] C. R. Zhang, "Improvement of genetic algorithm and optimization of grate cooler parameters," M.S. thesis, School Elect. Eng., Yanshan Univ., Yanshan, China, 2018.
[5] R. Kumar, L. A. Kumaraswamidhas, V. M. S. R. Murthy, and S. C. Vettivel, "Experimental investigations on machine vibration in blast-hole drills and optimization of operating parameters," *Measurement*, vol. 145, pp. 803–819, Oct. 2019.
[6] P. G. C. Manjunath and P. Krishna, "Prediction and optimization of dimensional shrinkage variations in injection molded parts using forward and reverse mapping of artificial neural networks," *Adv. Mater. Res.*, vols. 463–464, pp. 674–678, Feb. 2012.
[7] L. Gao, "The system of cement grate cooler thermal efficiency analysis and optimization guidance," M.S. thesis, School Automat. Elect. Eng., Jinan Univ., Jinan, China, 2016.
[8] Y. P. Liu and S. H. Ma, "Vehicle tranist time prediction based on multi-model fusion," *Comput. Mod.*, vol. 282, pp. 66–71 and 81, Feb. 2019.
[9] P. G. C. Manjunath, A. K. Shettigar, P. Krishna, and M. B. Parappagoudar, "Back propagation genetic and recurrent neural network applications in modelling and analysis of squeeze casting process," *Appl. Soft Comput.*, vol. 59, pp. 418–437, Oct. 2017.
[10] D. T. Zhang, "Research and implementation of imagequality quality assessment for spatial images," M.S. thesis, School Comput. Inf. Technol., Beijing Jiaotong Univ., Beijing, China, 2018.
[11] P. G. C. Manjunath, A. K. Shettigar, and M. B. Parappagoudar, "A systematic approach to model and optimize wear behaviour of castings produced by squeeze casting process," *J. Manuf. Process.*, vol. 32, pp. 199–212, Apr. 2018.
[12] H. O. Omoregbee and P. S. Heyns, "Fault classification of low-speed bearings based on support vector machine for regression and genetic algorithms using acoustic emission," *J. Vib. Eng. Technol.*, vol. 7, no. 5, pp. 455–464, Oct. 2019.
[13] P. G. C. Manjunath, P. Krishna, and M. B. Parappagoudar, "An intelligent system for squeeze casting process-soft computing based approach," *Int. J. Adv. Manuf. Technol.*, vol. 86, nos. 9–12, pp. 3051–3065, Oct. 2016.
[14] C. X. Ding, P. Zhang, X. F. Meng, W. J. Li, and Y. W. Wang, "On-line static voltage stability margin estimation based on classification regression tree algorithm," *Power Syst. Automat. J.*, vol. 31, pp. 1–14, Oct. 2019.
[15] Y. L. Xu, J. S. Zhang, X. Ji, B. B. Wang, and Z. F. Deng, "Research on short-term load forecasting method based on multi-model fusion neural network," *Control Eng.*, vol. 26, pp. 619–624, Apr. 2019.
[16] J. K. Kittur, G. C. M. Patel, and M. B. Parappagoudar, "Modeling of pressure die casting process: An artificial intelligence approach," *Int. J. Metalcasting*, vol. 10, no. 1, pp. 70–87, Jan. 2016.
[17] M. P. G. Chandrashekarappa, P. Krishna, and M. B. Parappagoudar, "Forward and reverse process models for the squeeze casting process using neural network based approaches," *Appl. Comput. Intell. Soft Comput.*, vol. 2014, pp. 152–163, Dec. 2014.

YUSEN GENG was born in Qingdao, Shandong, China, in 1993. He received the bachelor's degree in communication engineering from the University of Liaocheng, in 2017. He is currently pursuing the degree in control science and engineering with the University of Jinan.

His research interests include process industry automation control algorithm, industrial soft measurement, and integrated automation of process industry.

XIAOHONG WANG was born in Dezhou, Shandong, China, in 1963. He received the Ph.D. degree from Northeastern University, in 2005.

Since 2005, he has been the Director of the Shandong Provincial Comprehensive Automation Engineering Technology Research Center of Building Materials Industry. Since 2011, he has been the Director of the Shandong Provincial Key Laboratory of Comprehensive Automation of Building Materials Industry. He is currently a Professor with the School of Electronic and Engineering, University of Jinan. He is also a Taishan Scholar. His research interests include integrated automation of process industry, intelligent optimal control, and intelligent manufacturing standard. He is the Vice Chairman of the Shandong Automation Society.

PING JIANG was born in Heze, Shandong, China, in 1980. She received the Ph.D. degree in detection technology and automation device from Tianjin University.

From 2013 to 2017, she completed the Postdoctoral Research with Shandong University. She is currently an Associate Professor with the School of Electronic and Engineering, University of Jinan. She is the author of a great deal of research studies published at national and international journals, conference proceedings, as well as book chapters. Her research interests include image processing, fusion of multi-information, and process control of cement.